Available online at www.sciencedirect.com

ScienceDirect

Proceedings of the Combustion Institute 36 (2017) 1531–1538

Proceedings of the Combustion Institute

www.elsevier.com/locate/proci

Propagation speed and stability of spherically expanding hydrogen/air flames: Experimental study and asymptotics

Joachim Beeckmann [a,*], Raik Hesse [a], Stephan Kruse [a], André Berens [a], Norbert Peters [a], Heinz Pitsch [a], Moshe Matalon [b]

[a] *Institute for Combustion Technology, RWTH Aachen University, 52056 Aachen, Germany*
[b] *University of Illinois, Urbana-Champaign, United States*

Received 4 December 2015; accepted 30 June 2016
Available online 29 July 2016

Abstract

Here, outwardly propagating spherical hydrogen/air flames are examined theoretically and experimentally with respect to flame propagation speed and the onset of instabilities which develop due to thermal expansion and non-equal diffusivities. Instabilities increase the surface area of the spherical flame, and hence the flame propagation speed. The theory applied here accounts for both hydrodynamic and diffusive-thermal effects, incorporating temperature dependent transport coefficients. Experiments are performed in a spherical combustion chamber over a wide range of equivalence ratios (0.6–2.0), initial temperatures (298–423 K), and initial pressures (1 atm to 15 bar). The evolution of the flame propagation speed as a function of flame radius is compared to predictions from theory showing excellent agreement. Also the wrinkling of hydrogen/air flames is examined under increased pressure and temperature for various equivalence ratios. Critical flame radii, defined as the point of transition to cellular flames, are extracted from high-speed Schlieren flame imaging. Overall, the critical radius is found to decrease with increasing pressure. The predictions yield the growth rate of small disturbances and the critical flame radius. Experimental flame radii, as expected, are underpredicted by the theoretical findings. Experimental data are provided in the form of an approximation formula.

Keywords: Hydrogen; Laminar burning velocity; Spherical flames; Self-wrinkling flames; Hydrodynamic theory of flame propagation

1. Introduction

The response of flames to stretch, the stability characteristics of premixed flames, and the onset of cellular structures have been studied extensively in the past on the basis of asymptotic analysis [1–4]. The results are applicable to turbulent

* Corresponding author. Fax: +49 241 8092923.
E-mail address: jbeeckmann@itv.rwth-aachen.de (J. Beeckmann).

http://dx.doi.org/10.1016/j.proci.2016.06.194
1540-7489 © 2016 Published by Elsevier Inc. on behalf of The Combustion Institute.

flames in the flamelet regime [5,6]. Matalon et al. [7] extended the hydrodynamic theory considering also the effects of stoichiometry, variable transport coefficients, and arbitrary reaction orders. Numerical studies on the evolution of planar hydrogen flames with respect to instability effects were performed recently by Frouzakis et al. [8] and Altantzis et al. [9]. Strain rate effects on the non-linear development of aerodynamic unstable flames for planar and spherical flames were presented by Creta and Matalon [10]. Addabbo et al. [11] described the wrinkling of spherical expanding flames including variable transport. In addition, Bechtold et al. [12] included radiative losses. Also, Bradley and co-workers [13–15] as well as Law and co-workers [16,17] studied the transition from stable to cellular flames. Flame parameters such as flame thickness, global activation energy, and Lewis numbers must be properly extracted. For example, various definitions have been employed to evaluate the flame thickness, such as based on gradient, full width at half maximum, or by the thermal diffusivity of the combustible mixture [17].

Recently, Giannakopoulos et al. [18] discussed consistent definitions of flame displacement speed and Markstein length in the burnt, unburnt, and at any location within the preheat zone. Dahms investigated the early flame kernel growth in SI-engines, which is highly curved. In this study local Peclet numbers, defined as the flame radius divided by flame thickness, were assumed to be well below critical Peclet numbers related to the critical radius of a wrinkling flame. [19] This all underlines the importance of good, well-defined experimentally and/or theoretically obtained data of flame speed, Markstein length, and critical radii.

In this work, spherically expanding hydrogen/air flames are examined with special emphasis on flame propagation speed and instabilities. It is structured as follows: first, the experimental setup, the chemical mechanism, and simulation tools are described, followed by the extraction procedure of flame speed and Markstein length from experiments. Secondly, the theoretical framework for the estimation of flame displacement speed and the wrinkling of the flame by asymptotic theory is summarised from literature. Different types of flame surface appearance are categorised. Theoretical results of flame propagation speed over the radius are quantitatively compared to new experimental data, which has not been shown in previous literature, where typically qualitative comparisons were made [11]. Also, at present, experimental data on critical radii for hydrogen/air flames from literature are only available for temperatures of around 300 K and pressures of up to 10 bar. There is a lack of data for higher temperatures in combination with increased pressures. Here, experiments were performed over a wide range of equivalence ratios (0.5–2.0), initial temperatures (298 K to 423 K), and pressures (1 atm to 15 bar). Results

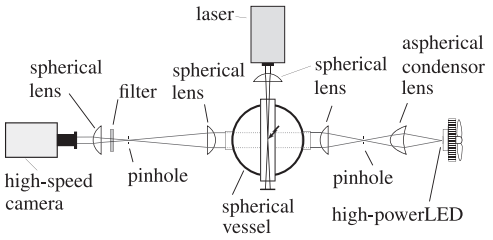

Fig. 1. Schematic of the experimental setup.

for altogether three kinds of critical radii are presented and compared with findings from the literature. Due to the utilisation of different flame thickness definitions in theoretical computation, only dimensional critical radii are presented here. Finally, the experiments are expressed by an approximation formula in the range of engine-like conditions representing early flame kernel growth in SI-engines. While the resulting expression is empirical, such fits can be quite useful and have often been used in numerical simulations.

2. Experimental and simulation framework

Experiments were performed in a high-pressure spherical combustion vessel. A schematic of the setup is shown in Fig. 1 and details are given in [20]. The location of the spherically propagating flame is imaged using a dual-field-lens Schlieren arrangement [21]. It is combined with a high-speed CMOS camera (LaVision HighSpeedStar 6). Images were taken with 25,000 frames per second (fps), at 448 × 448 pixels, and a resolution of 10.33 pixel/mm as well as with 16,000 fps, at 576 × 576 pixels, and a resolution of 14.23 pixel/mm in an earlier measurement campaign. A pulsed high-power LED of type Luminus CBT-120-G-C11-JK201 [22] is used. It emits light in a range of 530–535 nm. Optical lenses are an aspheric condenser lens and four spherical lenses. Two pinholes with a diameter of 0.5 mm are used. Overexposure of the camera from flame radiation is prevented by an optical filter.

The mixture preparation in a separate mixing vessel, the high-voltage coil discharge, and the ignition process are described in [20]. To allow laser ignition tests, an additional cylindrical spacer of 30 mm width is placed between the two half shells of the sphere with an inner diameter of 100 mm. The spacer is equipped with two rectangular quartz windows positioned on opposite sides. The optical access is 45 mm in height and 10 mm in width. The laser ignition is generated by a Lambda Physik EMG150 MSC excimer laser at a wavelength of 248 nm and energy of 200 mJ/pulse. The laser pulse is focused with a spherical lens in the middle of the vessel serving as a point ignition source. Experimental conditions were set up with hydrogen grade

6.0 and compressed air, which consists of 20.94% oxygen, 78.13% nitrogen, and 0.93% argon.

The experimentally deduced stretched flame propagation speed with respect to the burnt S_b can be determined from the Schlieren images by the derivative $\mathrm{d}r_f/\mathrm{d}t$ of flame radius r_f and time t. A least-squares fit through $S_b^0 - S_b = \mathcal{L}^b\kappa$ yields the unstretched flame speed S_b^0 and the burnt Markstein length $\mathcal{L}^b$ [3,18]. κ is the stretch rate, defined as the temporal change of a flame surface area A [23]. In addition, a non-linear extrapolation, discussed by Halter et al. [24], has been utilised yielding nearly the same results within the data range used for extrapolation.[1] Results are given for both methods in Table A.8 of the supplemental material. The laminar burning velocity S_L is determined from mass continuity through a planar unstretched flame, $S_\mathrm{L} = \rho_b/\rho_u \cdot S_b^0$.

A kinetic model for the oxidation of hydrogen by Hong et al. [27] is used for the calculation of physical properties, e.g. laminar burning velocities S_L, activation energies E, Lewis numbers Le, adiabatic flame temperatures T_b, unburnt ρ_u, and burnt mixture densities ρ_b. The FlameMaster software package [28] is used to obtain these numerical values.

3. Theoretical framework

A general description of the hydrodynamic theory of premixed flames of multidimensional structure in arbitrary flow fields has been published by Matalon et. al [7]. It is valid from lean to rich mixtures and allows for variable transport properties. The chemical reaction is defined by a single-overall irreversible global reaction step with two reactants, $\nu_\mathrm{E}\mathscr{M}_\mathrm{E} + \nu_\mathrm{D}\mathscr{M}_\mathrm{D} \rightarrow \mathit{Products}$, a deficient reactant with subscript D and an excess reactant with subscript E, the chemical symbol $\mathscr{M}_i$ stands for the single reactant and ν_i for its stoichiometric coefficient. Here, reaction orders are taken to be unity. A generalised form for arbitrary reaction orders is discussed in [7]. The mixture is characterised by two distinct Lewis numbers Le_E and Le_D, which are assumed constant. Analysis of the flame zone show that these two combine into a single effective Lewis number

$$Le_\mathrm{eff} = 1 + \frac{(Le_\mathrm{E} - 1) + (Le_\mathrm{D} - 1)\cdot\mathscr{A}}{1 + \mathscr{A}}, \tag{1}$$

with $\mathscr{A} = 1 + \beta(\Phi - 1)$ as a measure of the mixture's strength.[2] The parameter Φ is always defined larger than one; it is equal to the equivalence ratio ϕ for fuel-rich mixtures, and its reciprocal for fuel-lean mixtures. β is the Zeldovich number $\beta = E(T_b - T_u)/\mathcal{R}T_b^2$, with the universal gas constant $\mathcal{R}$ [31]. E can be determined from [32]

$$\frac{E}{\mathcal{R}} = -2\frac{\mathrm{d}\ln(\rho_u S_\mathrm{L})}{\mathrm{d}(1/T_b)}. \tag{2}$$

Evaluation of $E/\mathcal{R}$ requires the calculation of $\rho_u S_\mathrm{L}$ at different T_b. It is estimated by small variations of T_u [14]. The limiting Lewis numbers of the fuel and the oxidiser are calculated as 0.372 and 2.190. For lean and rich mixtures, the effective Lewis number tends towards the Lewis number of hydrogen and oxygen, respectively. It is a monotonically increasing function as the equivalence ratio increases from lean to rich.

3.1. Spherical flame propagation

Here, an outwardly propagating flame originating from an ignition point source is considered. The diffusion length, which also characterises the flame thickness $l_{f,\mathrm{D}}$, is defined as $l_{f,\mathrm{D}} \equiv D_\mathrm{th}/S_\mathrm{L} = \lambda/\rho_u c_p S_\mathrm{L}$. D_th is the thermal diffusivity of the combustible mixture. The velocity of the flame front $\dot{R}_f = \mathrm{d}R_f/\mathrm{d}t$, with the flame radius R_f, can be expressed by

$$\dot{R}_f = \sigma S_\mathrm{L} - \hat{\mathcal{L}}^b\mathbb{K}. \tag{3}$$

$\mathbb{K}$ and σ are the total stretch rate of the flame $\mathbb{K} = 2\sigma S_\mathrm{L}/R_f$ and the thermal expansion parameter $\sigma = \rho_u/\rho_b = T_b/T_u$, respectively [11]. The definition of the burnt Markstein number is given in [11] and also provided in the supplemental material.

3.2. Linear stability analysis

A theoretical description of the onset of instability in a spherically expanding flame was given in [33], where a Darrieus–Landau model with Markstein correction was considered, and later in [4], where, based on the hydrodynamic model, hydrodynamic and diffusive-thermal effects in a more systematic way were incorporated. The results were generalised in [11] to allow for temperature-dependent transport coefficients and a wider range of equivalence ratios. The spherical flame can be expressed by $r = R_f(t)$ with the propagation speed $\dot{R}_f$. The perturbed flame front can be written down in the form $r = R_f(t)[1 + \mathcal{A}(t)\mathbb{S}(\theta,\phi)]$, where $\mathcal{A}$ is the amplitude of the disturbance and $\mathbb{S}_n$ the spherical surface harmonics with n as an integer. According to [34], as the flame expands, the rate of growth/decay of the relative amplitude $\mathcal{A}(R_f)$ of a disturbance of wavenumber n is given by

$$\frac{1}{\mathcal{A}}\frac{\mathrm{d}\mathcal{A}}{\mathrm{d}t} = \frac{\dot{R}_f}{R_f}\left\{\omega_\mathrm{DL} - \frac{l_f}{R_f}\Omega\right\}, \tag{4}$$

[1] For larger lean premixed flames, DNS have indicated that stronger non-linearities in the extrapolation can be observed [25,26].

[2] A similar expression for Le_eff was also found by [29] and [30] carrying out stability analysis of a planar flame at near stoichiometric conditions.

$$\Omega = \Omega_1 + \frac{le_{\text{eff}}}{\sigma - 1}\Omega_2 + Pr\Omega_3. \quad (5)$$

The coefficients ω_{DL} and Ω depend on the thermal expansion σ, the reduced effective Lewis number $le_{\text{eff}} = \beta(Le_{\text{eff}} - 1)$, the Prandtl number Pr, and the wavenumber n. On the right hand side, ω_{DL} represents the destabilising effect of thermal expansion, whereas Ω represents the influence of thermal Ω_1, molecular Ω_2, and viscous Ω_3 diffusion. Definitions for ω_{DL} and Ω are given in [11] and the supplemental material.[3] Computations are based on a realistic choice of $Pr = 0.7$.

By discussing Eq. (4), a flame can only become unstable, if the growth rate of at least one wavenumber is positive. In general, by using adequate density ratios, coefficients ω_{DL} and $\Omega_{1,2,3}$ are positive. This means, without the stabilising effect of diffusion, in case of a positive coefficient Ω, a flame would be unstable at all times. The diffusion process can only turn negative if Le_{eff} is smaller than one. As described by [11], an instability occurs when the disturbance grows at a faster rate than the propagating flame. This point in time is defined as t_c. The instability can now be observed at a time $t_{\text{onset}} > t_c$. As an outcome of the theoretical stability analysis, t_c can be obtained, whereas for the comparison with experiments t_{onset} is of interest.

In order to determine t_c the mode growing first in Eq. (4) is considered as the most unstable one. It corresponds to $R_f = R_c$, which marks the onset of instability. A figure with the growth rate of several flame radii as a function of wavelength $\lambda = 2\pi R_f/n$ is given in the supplemental material for the same case discussed in the results section. At low radii the relevant wavelengths are limited by the highly curved flame and the short wavelength disturbances are stabilised by thermodiffusive effects. The flame becomes unstable when its radius exceeds a critical value and the long wavelength disturbances start growing as a result of hydrodynamic effects [4,34]. Marginal stability curves are obtained by setting the right-hand side of Eq. (4) to zero, leading to predictions for the critical flame radius, as shown in Fig. 4. The critical Peclet number $Pe_c = R_c/l_{f,\text{D}}$ depends only on the effective Lewis number and the gas thermal expansion. For hydrogen/air mixtures Pe_c decreases when the mixture is made leaner, and the instability onset occurs at a smaller radius. For a given mixture, i.e., fixed Le_{eff}, the critical radius R_c proportional to the flame thickness decreases with increasing pressure.

[3] There was a typographical error in the definition for Ω given in [11]. The first term ω^{-1} on the right hand side must be removed.

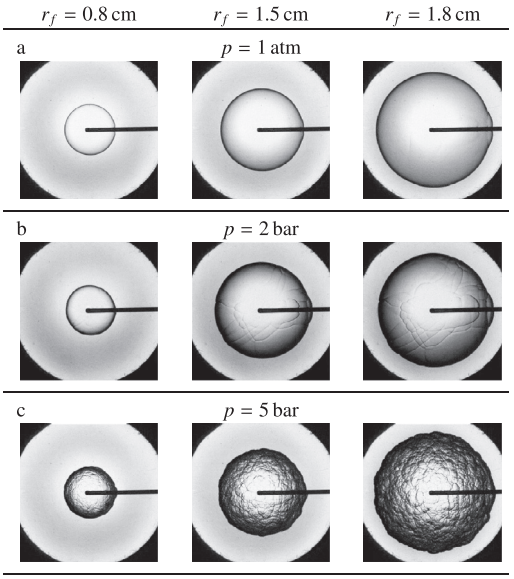

Fig. 2. Images of spherical hydrogen /air flames; $\phi = 1.0$ $T_i = 373$ K; smooth flame at 1 atm (a), with initial cracking at 2 bar (b), and with developed cellularity at 5 bar (c).

4. Results and discussion

Figure 2 shows the development of stoichiometric spherically expanding hydrogen/air flames at a temperature of 373 K and pressures of 1 atm, 2 bar, and 5 bar. The Schlieren images at atmospheric pressure show a smooth flame surface (Fig. 2a). Small cracks at the flame edge are associated with the flame passing across the spark electrodes, but do not alter flame speed. At 2 bar, however, first continuous cracking is observed (Fig. 2b). These cracks start to propagate and show initial cross-cracking, but no fully developed cellular structure. The start of cross-cracking can be interpreted as a critical (dimensional) radius $R_{c,1}$. At this stage the flame radius is bigger than the one evaluated by asymptotic theory. However, an influence on the flame displacement speed is not observed. At 5 bar the flame has a fully developed cellular structure already visible at the early stages of flame propagation (Fig. 2c). A significant number of new cells is formed with progressing flame evolution, accompanied by a significant increase in flame speed. In general, the influence of instabilities on the flame speed is identified by a sharp increase in propagation speed as stretch decreases. A critical flame radius $R_{c,2}$ can be identified [14].

Numerically and experimentally obtained mean values of $\bar{S}_{\text{L,exp}}$ used for the calculation of the flame propagation speed as a function of the radius are listed in Table 1. The propagation speed as a function of flame radius is shown in Fig. 3.

Table 1
Parameters used to evaluate propagation speed by asymptotic formulae for hydrogen/air mixtures at 298 K and 1 atm.

ϕ	T_b [K]	ρ_u [kg/m^3]	λ_u [W/mK]	c_p [J/kg K]	$\bar{S}_{\mathrm{L,exp}}$ [cm/s]	std [cm/s]	$\sigma = \frac{\rho_u}{\rho_b}$	$l_{f,\mathrm{D}}$ [mm]	Le_{eff}	Le^*_{eff}	E [kJ/mol]	β	α	α_{exp}
0.5	1637.8	0.977	0.0409	1201.38	58.77	0.24	5.02	0.0776	0.48	0.88	251.29	15.10	−11.80	−9.27
0.8	2168.4	0.893	0.0490	1313.82	157.96	0.55	6.38	0.0266	0.72	0.87	254.79	12.19	−3.80	1.19
1.0	2376.2	0.845	0.0538	1387.67	210.55	0.87	6.87	0.0215	1.24	0.87	268.11	11.87	11.82	14.55
1.5	2230.4	0.764	0.0624	1532.89	273.80	2.03	6.64	0.0193	1.81	0.80	167.74	7.84	19.94	22.24

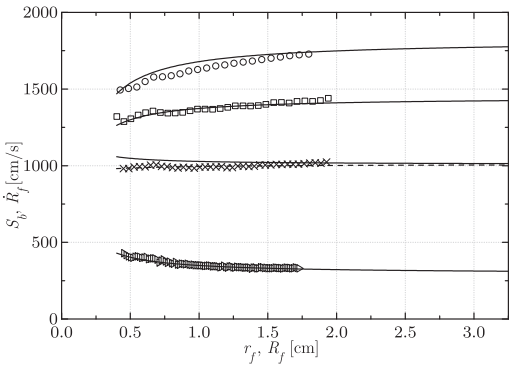

Fig. 3. Propagation speed of spherically expanding hydrogen/air flames as a function of flame radius at $p =$ 1 atm and $T = 298$ K for equivalence ratios of 0.5 ▷, 0.8 ×, 1.0 ○, and 1.5 □, calculated from asymptotic theory for reaction order unity ——, variable reaction orders – – –, and experiments (symbols).

Experimentally obtained data for S_b are shown for radii r_f up to 2 cm. Data for calculated $\dot{R}_f$ according to asymptotic theory are shown for radii R_f up to 3 cm. For the asymptotic formula the mean laminar flame speed from the experiments $\bar{S}_{\mathrm{L,exp}}$ is used. The burnt Markstein length changes sign when the effective Lewis number reaches a critical value $Le^*_{\mathrm{eff}} = 1 - 2\gamma_1/\sigma\beta\gamma_2$, which is slightly below one. When the effective Lewis number is bigger than its critical value $Le_{\mathrm{eff}} > Le^*_{\mathrm{eff}}$, the propagation speed increases as the flame grows larger. The reverse is true for $Le_{\mathrm{eff}} < Le^*_{\mathrm{eff}}$. Here, the critical effective Lewis number is estimated to 0.87 corresponding to an equivalence ratio of $\phi \approx 0.9$. For $\phi = 0.5$, 1.0, and 1.5, the experimental S_b and theoretical $\dot{R}_f$, as well as the experimental Markstein number α_{exp} and the parameter α obtained by dividing the theoretical Markstein length by the calculated flame thickness, are in excellent agreement. Only for $\phi = 0.8$, theory and experiments are deviating slightly. Experiments become slightly faster over the radius whereas theoretical results become slower. The effective Lewis number of 0.72 is estimated lower than the critical effective Lewis number, although it should be larger according to the experiments. One reason could be the assumption of reaction orders taken to be unity when calculating the effective Lewis number. Indeed, calculations of Le_{eff} with variable reaction orders taken from Sun et al. [35] and the generalised calculation of coefficient $\mathscr{A}$ from Matalon et al. [7] were performed for $\phi = 0.8$. The result agrees very well with the experiments and is shown as dashed line in Fig. 3. A theoretical Markstein number with a positive value of 1.99 is found. This is in accordance with an experimentally obtained Markstein number (positive value of 1.19). Using variable reaction orders for mixtures further away from the critical Lewis number do not show significant differences.

Next, hydrogen/air flame instabilities are examined. The critical radii R_{c}, $R_{\mathrm{c},1}$, and $R_{\mathrm{c},2}$ are determined experimentally and by asymptotic theory. For the following discussion, flames with an equivalence ratio of 1.8 are chosen at several pressures. As noted earlier, rich mixtures become unstable later than lean ones. This allows better discrimination of the critical radii in the experiments, but observations are still within optical accessibility of the spherical combustion vessel. The asymptotic computations do not consider radiative losses [12]. Radiation processes for the hydrogen/air flames have shown to be negligible at the conditions considered here, which is based on the findings by Varea et al. [26], Chen [36], and by Santner et al. [37]. Figure 4 shows the neutral stability curve in the n–Pe plane. Flame conditions are $p = 7.5$ bar and $T = 373$ K. The solid curve is obtained with effective Lewis numbers defined in Section 3. The nose of the peninsula determines the critical flame radius R_{c} and wave number n_{c} at the onset of instability yielding 2.20 mm and 13.4, respectively. The peninsula also describes the smallest and largest expected cell sizes by the asymptotes of its lower and upper branches. The largest expected cell sizes have a constant wave number n^* (lower branch)–destabilisation is only of hydrodynamic origin. The size scales linearly with the radius and is determined as $\lambda_{\mathrm{max}} = 2\pi R_f/n^*$. The asymptote of the upper branch is a line, $Pe/n = \Gamma$, with Γ depending on the effective Lewis number. The smallest cell size is determined as $\lambda_{\mathrm{min}} = 2\pi R_f/n \sim 2\pi\Gamma l_{f,D}$ and scales with the flame thickness [11,34]. In order to evaluate the sensitivity of the asymptotic theory, fuel and oxidiser Lewis numbers are taken from Sun et al. [35]. Basically, the changed effective Lewis number influences the size of the smallest cells (upper branch), but does not affect hydrodynamic instabilities (lower branch).

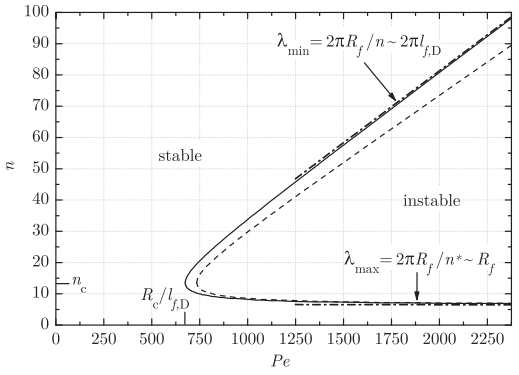

Fig. 4. Peninsula of unstable modes as a function of Pe of a hydrogen/air flame at $\phi = 1.8$, $p = 7.5$ bar, and $T = 373$ K, $Le_{eff} = 1.97$ ——, $Le_{eff} = 2.08$ – – –, asymptotes –·–·–.

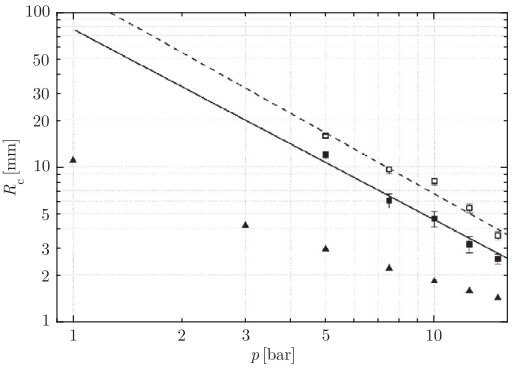

Fig. 6. Critical radii of hydrogen/air flames at $\phi = 1.8$, $T = 373$ K, and $p = 1$ atm–7.5 bar; $R_{c,1}$ ▪, $R_{c,2}$ ▫, Fit $R_{c,1}$ ——, Fit $R_{c,2}$ – – –, analytical solution ▲.

Below, the critical flame radii R_c are determined for different pressures, ranging from 1 to 15 bar, at an equivalence ratio of 1.8, and a temperature of 373 K. Numerical values as well as results for the evaluation of the critical radii by the asymptotic formulae are provided as supplemental material. In this work, the critical radii $R_{c,1}$ and $R_{c,2}$ of the experimental data are evaluated by an image post processing routine examining directly the flame images without determination of S_b and κ. In order to validate the processing routine, the criterion of a significant increase in flame speed for the definition of $R_{c,2}$ of the onset [13] is applied complementarily, yielding identical results for both routines. In addition, the influence of the spark plug as an ignition source and its orientation on the wrinkling has to be evaluated. The effect of spark plug orientation is examined while turning the spark plug in the vessel mounting by 90°. As a test condition 373 K, 7.5 bar, and $\phi = 1.8$ is chosen. Same results for $R_{c,1}$ and $R_{c,2}$ are obtained. A laser ignition setup is implemented as an alternative ignition source. Figure 5 shows a sequence of captured flame images with the laser ignition at the same test conditions. Until the flame reaches a radius of 1 cm, the flame surface remains smooth. Hereafter, first tiny disturbances can be identified. At a radius of 1.3 cm the entire flame surface is then covered by fully developed cells. The critical radius $R_{c,1}$ is not detectable due to the absence of initial cracks usually caused by the spark plug. To further verify the post processing routine, critical radii found in the literature are remeasured. The remeasured data at 5 bar and 298 K are in very good agreement with the original data from [17].

A comparison is now undertaken between the theoretical and experimental data obtained here. The results are compiled in Fig. 6. All three critical radii decrease linearly with increasing pressure. From the theory, it is clear that R_c must be smaller than the other two critical radii definitions. Unfortunately, it cannot be quantified how much smaller it has to be. Here, the theoretical findings are by a factor four to five smaller than the critical radii at t_{onset} and around three times smaller than $R_{c,1}$. In the literature, varying definitions for the flame thickness are given. The theoretical computations are obtained with the flame thickness defined by the laminar flame speed and diffusion. Increasing flame thickness would automatically increase the critical radius R_c. But it would not be accurate to arbitrarily change these parameters for the stability analysis, since they have proven to be of good choice for the evaluation of propagation speed. Nevertheless, for technical applications it is of

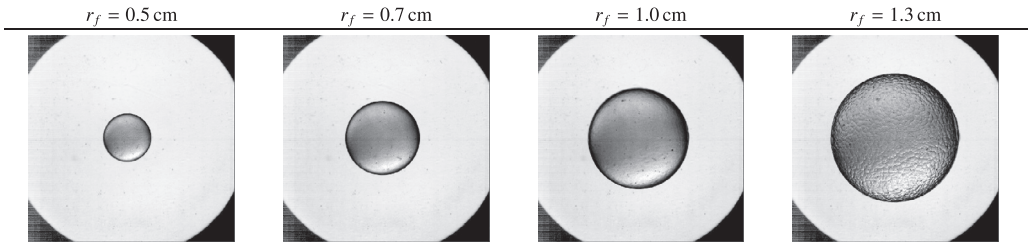

Fig. 5. Laser ignition of a hydrogen/air flame at $\phi = 1.8$, 7.5 bar, and 373 K.

Table 2
Coefficient of the approximation formula.

Case	$\mathcal{B}$	α	β	γ
$R_{c,1}$	0.9137	0.8146	−1.2336	1.2728
$R_{c,2}$	1.5225	0.8769	−1.2990	1.2384

interest to describe the evolution of the experimentally obtained critical radii by an approximation formula. The approximation formula is proposed as

$$\left(\frac{R_c}{R_{c,0}}\right) = \mathcal{B}\left(\frac{T}{T_0}\right)^{\alpha}\left(\frac{p}{p_0}\right)^{\beta}\left(\frac{\phi}{\phi_0}\right)^{\gamma}. \quad (6)$$

The critical radius $R_{c,0}$ of 12.5 mm from the $R_{c,1}$ data set is chosen as a normalisation parameter at $p_0 = 2.5$ bar, $T_0 = 373$ K, and $\phi_0 = 1.0$. The parameters $\mathcal{B}$, α, β, and γ are optimised over the full experimental range of 298–423 K, 2.5–15 bar, and equivalence ratios from 0.6 to 1.8. Altogether 31 data points for each approximation are used by least-square fitting. A separate set of data at $\phi = 1.0$, 423 K, and pressure ranging from 2.5 to 12.5 bar is used for validation. Results for the approximation formula for $R_{c,1}$ and $R_{c,2}$ are also incorporated in Fig. 6. Excellent agreement is achieved between experiments and the fit. Coefficients are summarised in Table 2.

5. Concluding remarks

In this work, the theory of flame propagation speed and stability is revisited. Flame parameters, like activation energy, Lewis numbers, thermal expansion (or heat release), and flame thickness play a significant role in asymptotic considerations of flame dynamics. First, it has been shown that the flame parameters chosen here result in propagation speed computations matching the experiments quantitatively very well. Also, comparison between Markstein numbers obtained by theory and experiment agree very well. Using the same flame parameters for stability considerations, the theoretical findings for the critical radii are always considerably lower than the experiment. This is to be expected because, although disturbances start growing when the flame reaches the size R_c, they do not grow initially as fast as the flame does and, moreover, the cells' amplitude must exceed a minimum size to be detected experimentally. The reverse trend reported in [17] is more likely due to a different interpretation of the parameters involved in the theoretical formulas. Therefore, a scaling of parameters sometimes also found in the literature, e.g. flame thickness, seems arbitrary and constraints for their applicability have to be carefully evaluated. The proposed approximation formula provides important information which can be used in early flame kernel propagation models in SI-engines.

Acknowledgements

This work was performed as part of the Cluster of Excellence "Tailor-Made Fuels from Biomass", which is funded by the Excellence Initiative of the German federal and state governments to promote science and research at German universities.

Supplementary material

Supplementary material associated with this article can be found, in the online version, at 10.1016/j.proci.2016.06.194.

References

[1] P. Clavin, F.A. Williams, *J. Fluid Mech.* 116 (1982) 251–282.
[2] P. Pelce, P. Clavin, *J. Fluid Mech.* 124 (1982) 219–237.
[3] M. Matalon, B.J. Matkowsky, *J. Fluid Mech.* 124 (1982) 239–259.
[4] J.K. Bechtold, M. Matalon, *Combust. Flame* 67 (1) (1987) 77–90.
[5] N. Peters, *Turbulent Combustion*, Cambridge University Press, 2000. Cambridge Books Online.
[6] N. Fogla, F. Creta, M. Matalon, *Combust. Flame* 162 (7) (2015) 2758–2777.
[7] M. Matalon, C. Cui, J.K. Bechthold, *J. Fluid Mech.* 487 (2003) 179–210.
[8] C.E. Frouzakis, N. Fogla, A.G. Tomboulides, C. Altantzis, M. Matalon, *Proc. Combust. Inst.* 35 (1) (2015) 1087–1095.
[9] C. Altantzis, C.E. Frouzakis, A.G. Tomboulides, M. Matalon, K. Boulouchos, *J. Fluid Mech.* 700 (2012) 329–361.
[10] F. Creta, M. Matalon, *Proc. Combust. Inst.* 33 (1) (2011) 1087–1094.
[11] R. Addabbo, J.K. Bechtold, M. Matalon, *Proc. Combust. Inst.* 29 (2) (2002) 1527–1535.
[12] J.K. Bechtold, C. Cui, M. Matalon, *Proc. Combust. Inst.* 30 (1) (2005) 177–184.
[13] D. Bradley, C.M. Harper, *Combust. Flame* 99 (3) (1994) 562–572.
[14] D. Bradley, R.A. Hicks, M. Lawes, C.G.W. Sheppard, R. Woolley, *Combust. Flame* 115 (1–2) (1998) 126–144.
[15] D. Bradley, C.G.W. Sheppart, R. Woolle, D.A. Greenhalgh, R.D. Lockett, *Combust. Flame* 122 (1) (2000) 195–209.
[16] C.K. Law, G. Jomaas, J.K. Bechtold, *Proc. Combust. Inst.* 30 (1) (2005) 159–167.
[17] G. Jomaas, C.K. Law, J.K. Bechtold, *J. Fluid Mech.* 583 (2007) 1–26.
[18] G.K. Giannakopoulos, A. Gatzoulis, C.E. Frouzakis, M. Matalon, A.G. Tomboulides, *Combust. Flame* 162 (4) (2015) 1249–1264.
[19] R. Dahms, *Modeling of Combustion in Spray-Guided Spark-Ignition Engines,* Ph.D. thesis, RWTH Aachen University, 2010.
[20] J. Beeckmann, L. Cai, H. Pitsch, *Fuel Part A* 117 (2014) 340–350.
[21] G.S. Settles, *Schlieren and Shadowgraph Techniques: Visualizing Phenomena in Transparent Media*, vol. 2, Springer, Berlin, 2001.

[22] Luminus DevicesInc., *CBT-120 Datasheet*, Luminus Devices, Inc., 2011.
[23] F.A. Williams, Combustion Theory: The Fundamental Theory of Chemically Reacting Flow Systems, Combustion Science and Engineering Series, Benjamin/Cummings Pub. Co., Menlo Park, California, 1985.
[24] F. Halter, T. Tahtouh, C. Mounaïm-Rousselle, *Combust. Flame* 157 (10) (2010) 1825–1832.
[25] F. Wu, W. Liang, Z. Chen, Y. Ju, C.K. Law, *Proc. Combust. Inst.* 35 (1) (2015) 663–670.
[26] E. Varea, J. Beeckmann, H. Pitsch, Z. Chen, B. Renou, *Proc. Combust. Inst.* 35 (1) (2015) 711–719.
[27] Z. Hong, D.F. Davidson, R.K. Hanson, *Combust. Flame* 158 (4) (2011) 633–644. Special Issue on Kinetics
[28] H. Pitsch, 1998. FlameMaster: A C++ computer program for 0D combustion and 1D laminar flame calculations
[29] G. Joulin, T. Mitani, *Combust. Flame* 40 (1981) 235–246.
[30] T.L. Jackson, *Combust. Sci. Technol.* 53 (1) (1987) 51–54.
[31] J.K. Bechtold, M. Matalon, *Combust. Flame* 127 (1–2) (2001) 1906–1913.
[32] N. Peters, F.A. Williams, *Combust. Flame* 68 (2) (1987) 185–207.
[33] A.G. Istratov, E.I. Korovjanskaja, V.B. Librovich, *Symp. (Int.) Combust.* 12 (1) (1969) 779–791.
[34] M. Matalon, *Annu. Rev. Fluid Mech.* 39 (2007) 163–191.
[35] C.J. Sun, C.J. Sung, L. He, C.K. Law, *Combust. Flame* 118 (1–2) (1999) 108–128.
[36] Z. Chen, *Combust. Flame* 157 (2010) 2267–2276.
[37] J. Santner, F.M. Haas, Y. Ju, F.L. Dryer, *Combust. Flame* 161 (1) (2014) 147–153.